Simulating Exceptional Non-Hermitian Metals with Single-Photon Interferometry

Kunkun Wang,[1,5] Lei Xiao,[1] Jan Carl Budich,[2,*] Wei Yi,[3,4,†] and Peng Xue[1,‡]
[1]Beijing Computational Science Research Center, Beijing 100084, China
[2]Institute of Theoretical Physics, Technische Universität Dresden and Würzburg-Dresden Cluster of Excellence ct.qmat, 01062 Dresden, Germany
[3]CAS Key Laboratory of Quantum Information, University of Science and Technology of China, Hefei 230026, China
[4]CAS Center For Excellence in Quantum Information and Quantum Physics, Hefei 230026, China
[5]School of Physics and Material Science, Anhui University, Hefei 230601, China

(Received 2 October 2020; revised 8 April 2021; accepted 9 June 2021; published 9 July 2021)

We experimentally simulate in a photonic setting non-Hermitian (NH) metals characterized by the topological properties of their nodal band structures. Implementing nonunitary time evolution in reciprocal space followed by interferometric measurements, we probe the complex eigenenergies of the corresponding NH Bloch Hamiltonians, and study in detail the topology of their exceptional lines (ELs), the NH counterpart of nodal lines in Hermitian systems. We focus on two distinct types of NH metals: two-dimensional systems with symmetry-protected ELs, and three-dimensional systems possessing symmetry-independent topological ELs in the form of knots. While both types feature open Fermi surfaces, we experimentally observe their distinctions by analyzing the impact of symmetry-breaking perturbations on the topology of ELs.

DOI: 10.1103/PhysRevLett.127.026404

Introduction.—Phases of quantum matter characterized by topologically robust nodal band structures, such as Weyl semimetals exhibiting remarkable transport properties [1], have been a major focus of both theoretical and experimental study for the past decade [1–6]. Recently, it has become clear that non-Hermiticity, a common element in open, dissipative systems [7–10], can qualitatively modify key features of band topology (see Ref. [6] for a review). This leads to a variety of fascinating phenomena, including the emergence of anomalous topological edge states [11–18], and the presence of exceptional lines (ELs) [19], the non-Hermitian (NH) generalization of nodal lines along which the NH Hamiltonian is nondiagonalizable [20–30]. In particular, at least two distinct classes of NH metals have been theoretically identified, one with ELs protected by NH symmetries that reduce the codimension of exceptional points (EPs) [23,31], the other featuring nodal band structures and knotted ELs with intrinsic, symmetry-independent topology [24]. These NH metals are in sharp contrast to their Hermitian, semimetal counterparts, where ELs and Fermi surfaces are reduced to isolated Weyl points and surface Fermi arcs, respectively [32–36]. While nodal band structures in both Hermitian and NH settings have seen a great surge of experimental interest recently [37–42], a systematic study of unconventional NH metals and their topological stability is still lacking.

In this work, we experimentally simulate and observe NH metals using single-photon interferometry (see Fig. 1 for an illustration of our setup), with a particular focus on the stability and topology of the ELs with respect to perturbations. Experimentally, this is achieved by implementing nonunitary time evolution for single photons that is governed by a corresponding NH Hamiltonian, and by performing interferometric measurements on the photons to extract the complex eigenenergies for each mode in reciprocal space. We simulate both NH metals featuring

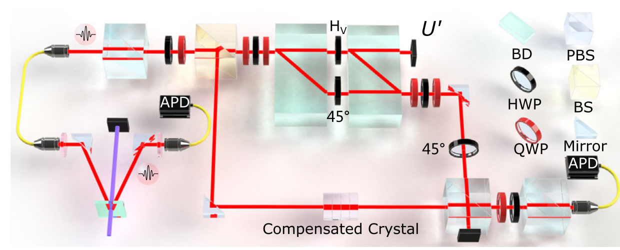

FIG. 1. Experimental setup. The polarization of the signal photon generated by the standard spontaneous parametric down-conversion is projected into the polarization state $|\psi_\pm\rangle$ with a polarizing beam splitter (PBS), a half-wave plate (HWP), and a quarter-wave plate (QWP), and then goes through the interferometric network. After passing through a 50:50 beam splitter (BS), the photon is either transmitted or reflected, and thus separated into different paths. Subsequently, a nonunitary operation U' realized via sets of wave plates and two beam displacers (BDs) is performed on its polarization state in the transmitted mode which acquires a complex phase shift, corresponding to the eigenenergies of H'. Finally, the photon is detected by avalanche photodiodes (APDs) resulting in a "click click" in coincidence detection event involving another trigger photon. We measure the eigenenergies in momentum space via interferometric measurements.

symmetry-protected ELs in two-dimensional (2D) systems and knotted ELs including a trefoil knot in three-dimensional (3D) systems, thus observing how EPs may form closed lines and even knots in momentum space.

More specifically, for symmetry-protected NH models in 2D, we show that the closed exceptional-line structures bound open Fermi volumes, and are robust against symmetry-preserving perturbations, while symmetry-breaking terms generically remove the ELs. This is in contrast to their 2D Hermitian analogs, where nodal points occur only at isolated momenta and do not give rise to bulk Fermi volumes. We further simulate 3D NH metals with both knotted and linked ELs that bound open Fermi surfaces representing the topological Seifert-surfaces of the corresponding knots [24]. There, observing the robustness of the band-structure topology with respect to generic perturbations, we confirm the topological stability of nodal knots in NH systems. Our results thus experimentally establish the topological variety and stability of nodal structures in NH metals.

Theoretical framework.—We consider two-band NH metals, as described in reciprocal space by the NH Bloch Hamiltonian

$$H(\mathbf{k}) = \mathbf{d}_R(\mathbf{k}) \cdot \boldsymbol{\sigma} + i\mathbf{d}_I(\mathbf{k}) \cdot \boldsymbol{\sigma}, \tag{1}$$

where $\boldsymbol{\sigma}$ are the standard Pauli matrices, $\mathbf{k}$ is the lattice momentum for either a 2D or 3D lattice model, with the complex Bloch vector $\mathbf{d} = \mathbf{d}_R + i\mathbf{d}_I$, where $\mathbf{d}_R, \mathbf{d}_I \in \mathbb{R}^3$. With the eigenvalues of the NH Bloch Hamiltonian (1) given by $E_\pm = \pm\sqrt{d_R^2 - d_I^2 + 2i\mathbf{d}_R \cdot \mathbf{d}_I}$, EPs occur whenever eigenvalues coalesce ($E_+ = E_-$) at nonvanishing $\mathbf{d}$, i.e., for nontrivial solutions to the equations $d_R^2 - d_I^2 = 0$ and $\mathbf{d}_R \cdot \mathbf{d}_I = 0$ [43]. Depending on the presence of NH symmetries as well as the spatial dimension of the system, the EPs can form closed ELs in the reciprocal space, with either symmetry-protected, or symmetry-independent topology. Specifically, ELs independent of symmetry occur in 3D, while suitable NH symmetries may reduce the codimension of EPs by one, thus stabilizing ELs in 2D systems. In both cases, ELs constitute boundaries for open Fermi volumes or surfaces, characterized by vanishing real parts of the energy gap, thus giving rise to symmetry-protected or intrinsic NH metals. Besides their topological stability, ELs in 3D may be topologically distinguished by forming different knots [24].

For the symmetry-protected NH metal, we consider a model on a 2D square lattice with unit lattice constant preserving the NH symmetry

$$H = qH^\dagger q^{-1}, \qquad q^\dagger q^{-1} = qq^\dagger = \mathbb{1}. \tag{2}$$

By taking $q = \sigma_x$, the relation $\mathbf{d}_R \cdot \mathbf{d}_I = 0$ is satisfied automatically [23]. The ELs are therefore defined and tunable as closed contours in 2D momentum space that satisfy the single constraint $d_R^2 - d_I^2 = 0$. In particular, the parameter space is divided into regions with entirely real and entirely imaginary eigenspectrum, with ELs forming the boundary between the two.

By contrast, in three dimensions, the solutions of $\mathrm{Re}(E^2) = 0$ and $\mathrm{Im}(E^2) = 0$ each yield a closed 2D surface in 3D momentum space, and these two hyperplanes generically intersect at topologically stable closed lines in the parameter space, thus giving rise to NH metals with ELs that are robust against symmetry-breaking perturbations. These ELs with intrinsic topology can form knots or links in reciprocal space, and are thus fundamentally distinct from symmetry-protected ELs in 2D.

Experimental simulations.—We observe both symmetry-protected and intrinsic ELs by simulating the corresponding NH Bloch Hamiltonians $H(\mathbf{k})$ in reciprocal space, and by measuring the complex eigenenergies $E_\pm(\mathbf{k})$ using single-photon interferometry. While an arbitrary NH dynamic is difficult to implement experimentally due to the difficulty of achieving gain in quantum systems [44], especially with single photons, we circumvent this difficulty through a mapping

$$H'(\mathbf{k}) = H(\mathbf{k}) + d_0\sigma_0, \tag{3}$$

where σ_0 is the 2×2 identity matrix, and $d_0 = i \ln \sqrt{1/\Lambda}$, with $\Lambda = \max_{\mathbf{k}} |\lambda_{\mathbf{k}}|$ and $\lambda_{\mathbf{k}}$ the eigenvalue of $e^{-iH}e^{-iH^\dagger}$ [45,46]. It follows that H and H' have the same eigenstates, while eigenenergies of H' are related to those of H through $E'_\pm = E_\pm - i \ln \sqrt{\Lambda}$.

As a general framework, we encode the basis states into the orthogonal polarization states of a single photon, and initialize the polarization state in $|\psi_\pm\rangle$, the eigenstates of $H'(\mathbf{k})$ of a given $\mathbf{k}$ sector. We then send the photon through a 50:50 beam splitter, after which the photon is in the state

$$|\Psi_j\rangle = \frac{1}{\sqrt{2}}(|\psi_j\rangle|t\rangle + |\psi_j\rangle|r\rangle), \qquad (j = \pm), \tag{4}$$

where t and r denote the transmitted and reflected modes of the single photon, respectively. The nonunitary time evolution governed by $e^{-iH'}$ is selectively enforced on the transmitted photon, leading to the state

$$\begin{aligned} |\Psi'_j\rangle &= (e^{-iH'} \otimes |t\rangle\langle t| + \mathbb{1} \otimes |r\rangle\langle r|)|\Psi_j\rangle \\ &= \frac{1}{\sqrt{2}}(e^{-iE'_j}|\psi_j\rangle|t\rangle + |\psi_j\rangle|r\rangle), \end{aligned} \tag{5}$$

from which E'_j is extracted through an interferometric measurement [47].

Symmetry-protected ELs.—We first simulate the following 2D NH Hamiltonian with symmetry-protected ELs

$$H_1 = (2 - \cos k_x - \cos k_y)\sigma_x + \frac{i}{4}\sigma_z. \tag{6}$$

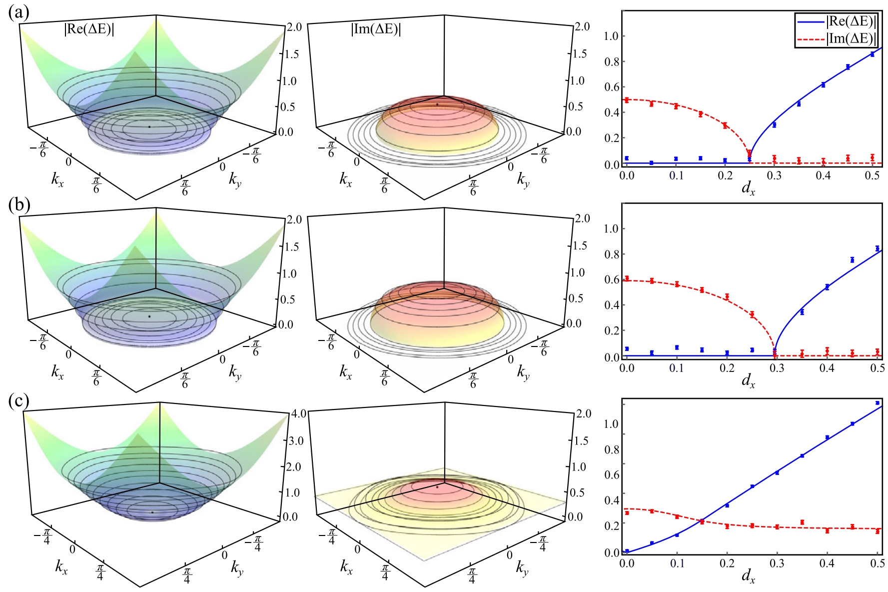

FIG. 2. Observation of symmetry-protected ELs. (a) The real (left column) and imaginary (middle column) parts of the spectral gaps ΔE as a function of momentum for the symmetry-protected NH metal H_1. Experimental data are shown as black lines and theoretical results are shown as colored contour plots. Right column: the real and imaginary parts of the energy gap ΔE as a function of the parameter d_x. Theoretical predictions are represented by lines, and the experimental results by symbols. Error bars are obtained by assuming Poisson statistics in the photon-number fluctuations, indicating the statistical uncertainty. Effects due to the symmetry-preserving perturbation $i(\pi/20)\sigma_y$ and the symmetry-broken perturbation $i(\pi/20)\sigma_x$ are shown in (b) and (c), respectively.

Note that H_1 satisfies the symmetry defined in Eq. (2). We sample 11 different Bloch vectors $d_x = 2 - \cos k_x - \cos k_y$, and measure the eigenenergies of both bands. Each sampled d_x corresponds to a closed loop in the Brillouin zone that has the same eigenenergy. In Fig. 2(a), we show the real and imaginary components of the energy gap $\Delta E = E_+ - E_-$ in momentum space, which agree well with theoretical predictions. Particularly, an exceptional

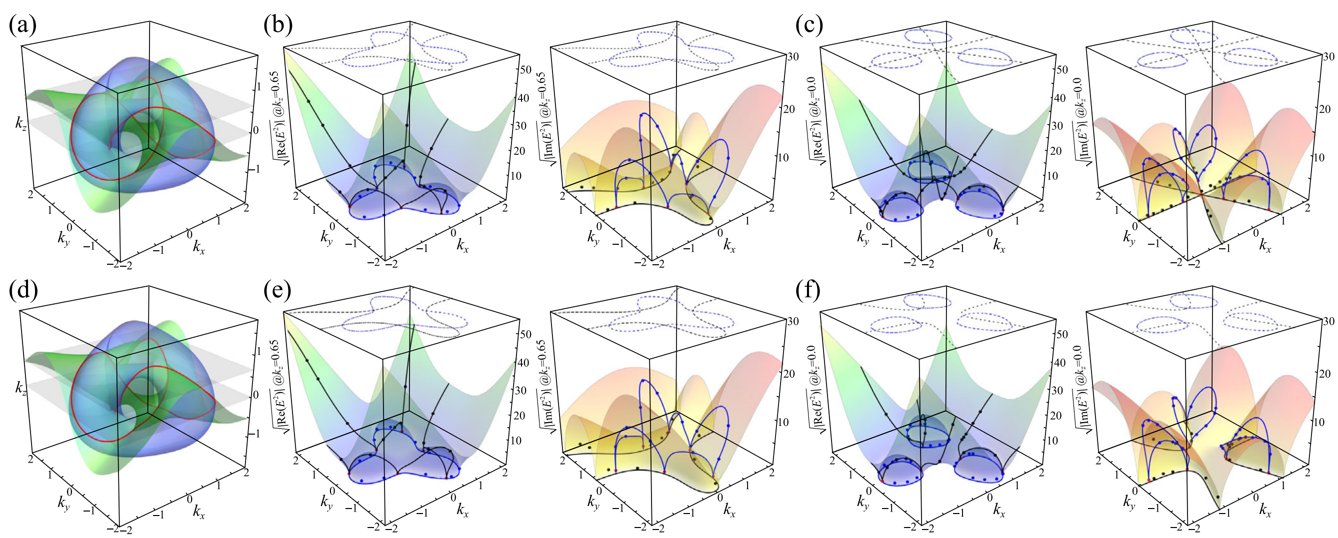

FIG. 3. Observation of symmetry-independent knotted ELs. (a) Blue and green surfaces correspond to $\mathrm{Re}(E^2) = 0$ and $\mathrm{Im}(E^2) = 0$, respectively. The solid red curve is trefoil knotted EL, i.e., the intersection of two surfaces. Two gray planes correspond to the surfaces with $k_z = 0.65$ and 0, respectively, which are chosen in our experiment. $\sqrt{|\mathrm{Re}(E^2)|}$ and $\sqrt{|\mathrm{Im}(E^2)|}$ with fixed $k_z = 0.65$ (b) and $k_z = 0$ (c) as functions of k_x and k_y. Solid black curves are the intersections between the surfaces $\mathrm{Im}(E^2) = 0$ and the gray planes. Blue solid curves are the intersections between the surfaces $\mathrm{Re}(E^2) = 0$ and the gray planes. EPs correspond to intersections of black and blue curves. Experimental data are shown as the black, blue, and red dots, and theoretical results are shown as the colored curves and the colored contour plots. (d)–(f) Effects of perturbations $\sum_{i=x,y,z} \delta_i \sigma_i$, where $\delta_i \in [0, 0.4]$ are chosen randomly. In our experiment, we have $\delta_x = 0.3179$, $\delta_y = 0.3590$, and $\delta_z = 0.2211$.

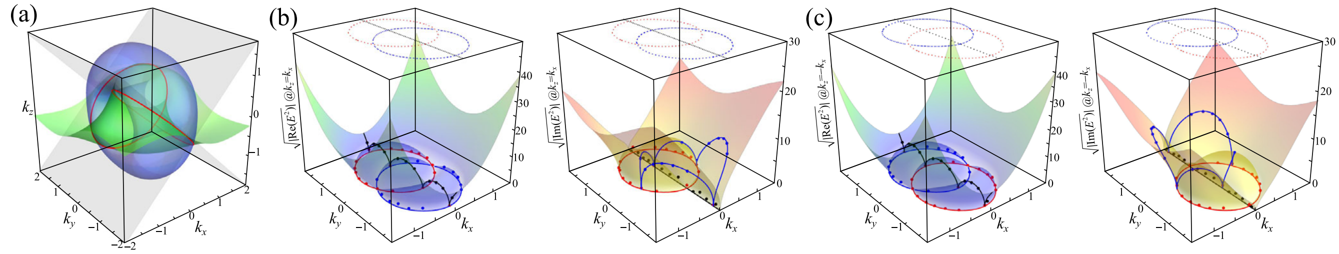

FIG. 4. Observation of linked ELs. (a) Blue and green surfaces correspond to $\mathrm{Re}(E^2) = 0$ and $\mathrm{Im}(E^2) = 0$, respectively. The solid red curves correspond to the Hopf linked ELs, i.e., the intersection of two surfaces. The gray planes are the surfaces with $k_z = k_x, -k_x$, respectively, which are chosen in our experiment. $\sqrt{|\mathrm{Re}(E^2)|}$ and $\sqrt{|\mathrm{Im}(E^2)|}$ with fixed $k_z = k_x$ (b) and $k_z = -k_x$ (c) as functions of k_x and k_y. Solid black curves are the intersections between the surfaces $\mathrm{Im}(E^2) = 0$ and the gray planes. Blue solid curves are the intersections between the surfaces $\mathrm{Re}(E^2) = 0$ and the gray planes. Red solid curves and the intersections of black and blue curves are ELs and EPs corresponding to the intersections between the Hopf link and the gray planes. The experimental data are shown as the black, blue, and red dots, and theoretical results are shown as the colored curves and the colored contour plots.

ring exists at $d_x = 0.25$, by which the parameter space is divided into regions with either real or purely imaginary eigenenergies. It follows that the exceptional ring serves as a boundary for the open Fermi volume with $\mathrm{Re}(\Delta E) = 0$, i.e., an open set with the same dimensionality as the bulk system. As a defining signature of symmetry protection, the topology of the exceptional ring is robust against symmetry-preserving perturbations. This is illustrated in Fig. 2(b), where the exceptional ring persists but is shifted in parameter space (now at $d_x = 0.295$), upon the addition of a small perturbative term of the form $i(\pi/20)\sigma_y$. By contrast, when a symmetry-breaking perturbation of the form $i(\pi/20)\sigma_x$ is added [see Fig. 2(c)], EPs disappear, in accordance with theoretical predictions. Generalizing this strategy, we are able to experimentally simulate the general class of NH models with symmetry-protected ELs [47].

Symmetry-independent knotted ELs.—We now turn to NH models with symmetry-independent ELs. Following Ref. [24], we construct models with intrinsic knotted or linked ELs in momentum space. This is achieved by taking

$$\mathbf{d}_R(\mathbf{k}) = [f_1(\mathbf{k}) - \epsilon, \epsilon, 0], \quad \mathbf{d}_I(\mathbf{k}) = [0, f_2(\mathbf{k}), \sqrt{2}\epsilon] \tag{7}$$

in Eq. (1), where $f_{1,2}(\mathbf{k})$ are real and continuous scalar functions constrained by $f_1(\mathbf{k}) + i f_2(\mathbf{k}) = Z_0^p + Z_1^q$, with $(Z_0, Z_1) \in \mathbb{C}^2$ and $|Z_0|^2 + |Z_1|^2 = 1$. Here, ϵ is a constant with sufficiently large amplitude, which is fixed as $\epsilon = -20$ for our work. By construction, if (p, q) are coprime (both even) integers, a NH Hamiltonian with Bloch vectors satisfying Eq. (7) features ELs with (p, q) knot (link) topology.

For our experiment, we adopt the construction

$$Z_0 = \sin k_x + i \sin k_y,$$
$$Z_1 = 2 \sum_{\alpha = x,y,z} \cos k_\alpha - 5 + i \sin k_z \tag{8}$$

to generate the functions f_1 and f_2 (such a construction is not unique though). First, we solve f_1 and f_2 using $(p, q) = (3, 2)$, and simulate the corresponding NH Hamiltonian with trefoil-knotted ELs [see Fig. 3(a)]. In Figs. 3(b) and 3(c), we show the measured $\sqrt{|\mathrm{Re}(E^2)|}$ and $\sqrt{|\mathrm{Im}(E^2)|}$ with fixed $k_z = 0.65$ (b) and $k_z = 0$ (c) as functions of k_x and k_y, which agree well with the corresponding theoretical values and reveal the underlying knotted topology of the ELs. In this case, the knotted ELs serve as the boundary for the topologically nontrivial open Fermi-Seifert surface defined by $\mathrm{Re}(E) = 0$ [24].

To investigate the robustness of ELs, we introduce a general, symmetry-breaking perturbation $\sum_{i=x,y,z} \delta_i \sigma_i$, where $\delta_i \in [0, 0.4]$ are chosen randomly. The experimental data shown in Figs. 3(d)–3(f) correspond to the coefficients $\delta_x = 0.3179$, $\delta_y = 0.3590$, and $\delta_z = 0.2211$. With the addition of perturbations, the knotted ELs still exist [see Figs. 3(d)–3(f)], while their shapes are slightly deformed compared to those without perturbations. These observations experimentally confirm and exemplify the robustness of knotted ELs to generic perturbations.

As a second case of NH model with intrinsic ELs, we adopt the same construction (8), but with $(p, q) = (2, 2)$. The resulting NH Hamiltonian features ELs with a link geometry [see Fig. 4(a)]. The experimentally measured $\sqrt{|\mathrm{Re}(E^2)|}$ and $\sqrt{|\mathrm{Im}(E^2)|}$ with $k_z = \pm k_x$ are shown in Figs. 4(b) and 4(c). Similar to the knotted ELs, the linked topology here is also found to be robust to generic perturbations.

Conclusion.—By simulating and observing two different classes of NH metals, our present experimental study corroborates the topological robustness of ELs that occur in a rich variety of nodal NH band structures. While our findings hopefully inspire the investigation of exotic NH metals also in other physical platforms, we note that our present experimental scheme may readily be extended to multiband models and systems with other symmetries, thus offering a versatile toolbox for the systematic experimental study of nodal phases in both Hermitian and non-Hermitian settings. Furthermore, our configuration enables the investigation of dynamical properties of NH metals, where the presence of open Fermi volumes or open Fermi surfaces may give rise to so far unexplored phenomena.

We acknowledge fruitful discussions with Emil J. Bergholtz. This work has been supported by the National Natural Science Foundation of China (Grants No. 12025401, No. 11974331, and No. U1930402). L. X, acknowledges support from the project funded by China Postdoctoral Science Foundation (Grant No. 2020M680006). W. Y. acknowledges support from the National Key Research and Development Program of China (Grants No. 2016YFA0301700 and No. 2017YFA0304100). J. C. B. acknowledges financial support from the German Research Foundation (DFG) through the Collaborative Research Centre SFB 1143 (project ID 247310070) and the Cluster of Excellence ct.qmat (EXC 2147, project ID 390858490).

[*]jan.budich@tu-dresden.de
[†]wyiz@ustc.edu.cn
[‡]gnep.eux@gmail.com

[1] N. P. Armitage, E. J. Mele, and A. Vishwanath, Weyl and Dirac semimetals in three-dimensional solids, Rev. Mod. Phys. **90**, 015001 (2018).
[2] M. Z. Hasan and C. L. Kane, Topological insulators, Rev. Mod. Phys. **82**, 3045 (2010).
[3] X.-L. Qi and S.-C. Zhang, Topological insulators and superconductors, Rev. Mod. Phys. **83**, 1057 (2011).
[4] T. O. Wehling, A. M. Black-Schaffer, and A. V. Balatsky, Dirac materials, Adv. Phys. **63**, 1 (2014).
[5] T. Ozawa, H. M. Price, A. Amo, N. Goldman, M. Hafezi, L. Lu, M. C. Rechtsman, D. Schuster, J. Simon, O. Zilberberg, and I. Carusotto, Topological photonics, Rev. Mod. Phys. **91**, 015006 (2019).
[6] E. J. Bergholtz, J. C. Budich, and F. K. Kunst, Exceptional topology of non-Hermitian systems, Rev. Mod. Phys. **93**, 015005 (2021).
[7] C. M. Bender and S. Boettcher, Real Spectra in non-Hermitian Hamiltonians Having $\mathcal{PT}$ Symmetry, Phys. Rev. Lett. **80**, 5243 (1998).
[8] C. M. Bender, D. C. Brody, and H. F. Jones, Complex Extension of Quantum Mechanics, Phys. Rev. Lett. **89**, 270401 (2002).
[9] C. M. Bender, Making sense of non-Hermitian Hamiltonians, Rep. Prog. Phys. **70**, 947 (2007).
[10] R. El-Ganainy, K. G. Makris, M. Khajavikhan, Z. H. Musslimani, S. Rotter, and D. N. Christodoulides, Non-Hermitian physics and $\mathcal{PT}$ symmetry, Nat. Phys. **14**, 11 (2018).
[11] T. E. Lee, Anomalous Edge State in a non-Hermitian Lattice, Phys. Rev. Lett. **116**, 133903 (2016).
[12] L. Xiao, X. Zhan, Z. H. Bian, K. K. Wang, X. Zhang, X. P. Wang, J. Li, K. Mochizuki, D. Kim, N. Kawakami, W. Yi, H. Obuse, B. C. Sanders, and P. Xue, Observation of topological edge states in parity–time-symmetric quantum walks, Nat. Phys. **13**, 1117 (2017).
[13] F. K. Kunst, E. Edvardsson, J. C. Budich, and E. J. Bergholtz, Biorthogonal Bulk-Boundary Correspondence in non-Hermitian Systems, Phys. Rev. Lett. **121**, 026808 (2018).
[14] Y. Xiong, Why does bulk boundary correspondence fail in some non-Hermitian topological models, J. Phys. Commun. **2**, 035043 (2018).
[15] S. Yao and Z. Wang, Edge States and Topological Invariants of non-Hermitian Systems, Phys. Rev. Lett. **121**, 086803 (2018).
[16] L. Xiao, T. Deng, K. Wang, G. Zhu, Z. Wang, W. Yi, and P. Xue, Non-Hermitian bulk-boundary correspondence in quantum dynamics, Nat. Phys. **16**, 761 (2020).
[17] N. Okuma, K. Kawabata, K. Shiozaki, and M. Sato, Topological Origin of non-Hermitian Skin Effects, Phys. Rev. Lett. **124**, 086801 (2020).
[18] X. Zhang, G. J. Li, Y. H. Liu, T. Tai, R. Thomale, and C. H. Lee, Tidal surface states as fingerprints of non-Hermitian nodal knot metals, Commun. Phys. **4**, 47 (2021).
[19] X. Zhang, K. Ding, X. Zhou, J. Xu, and D. Jin, Experimental Observation of an Exceptional Surface in Synthetic Dimensions with Magnon Polaritons, Phys. Rev. Lett. **123**, 237202 (2019).
[20] Y. Xu, S.-T. Wang, and L.-M. Duan, Weyl Exceptional Rings in a Three-Dimensional Dissipative Cold Atomic Gas, Phys. Rev. Lett. **118**, 045701 (2017).
[21] R. A. Molina and J. González, Surface and 3D Quantum Hall Effects from Engineering of Exceptional Points in Nodal-Line Semimetals, Phys. Rev. Lett. **120**, 146601 (2018).
[22] J. Carlström and E. J. Bergholtz, Exceptional links and twisted Fermi ribbons in non-Hermitian systems, Phys. Rev. A **98**, 042114 (2018).
[23] J. C. Budich, J. Carlström, F. K. Kunst, and E. J. Bergholtz, Symmetry-protected nodal phases in non-Hermitian systems, Phys. Rev. B **99**, 041406(R) (2019).
[24] J. Carlström, M. Stålhammar, J. C. Budich, and E. J. Bergholtz, Knotted non-Hermitian metals, Phys. Rev. B **99**, 161115(R) (2019).
[25] Z. Yang and J. Hu, Non-Hermitian Hopf-link exceptional line semimetals, Phys. Rev. B **99**, 081102(R) (2019).
[26] H. Wang, J. Ruan, and H. Zhang, Non-Hermitian nodal-line semimetals with an anomalous bulk-boundary correspondence, Phys. Rev. B **99**, 075130 (2019).
[27] K. Kawabata, T. Bessho, and M. Sato, Classification of Exceptional Points and non-Hermitian Topological Semimetals, Phys. Rev. Lett. **123**, 066405 (2019).
[28] Z. Yang, C.-K. Chiu, C. Fang, and J. Hu, Jones Polynomial and Knot Transitions in Hermitian and non-Hermitian Topological Semimetals, Phys. Rev. Lett. **124**, 186402 (2020).
[29] C. H. Lee, A. Sutrisno, T. Hofmann, T. Helbig, Y. Liu, Y. S. Ang, L. K. Ang, X. Zhang, M. Greiter, and R. Thomale, Imaging nodal knots in momentum space through topolectrical circuits, Nat. Commun. **11**, 4385 (2020).
[30] A. Banerjee and A. Narayan, Non-Hermitian semi-Dirac semi-metals, J. Phys. Condens. Matter **33**, 225401 (2021).
[31] T. Yoshida, R. Peters, N. Kawakami, and Y. Hatsugai, Symmetry-protected exceptional rings in two-dimensional correlated systems with chiral symmetry, Phys. Rev. B **99**, 121101(R) (2019).

[32] C. Fang, H. Weng, X. Dai, and Z. Fang, Topological nodal line semimetals, Chin. Phys. B **25**, 117106 (2016).

[33] R. Bi, Z. Yan, L. Lu, and Z. Wang, Nodal-knot semimetals, Phys. Rev. B **96**, 201305(R) (2017).

[34] M. Ezawa, Topological semimetals carrying arbitrary Hopf numbers: Fermi surface topologies of a Hopf link, Solomon's knot, trefoil knot, and other linked nodal varieties, Phys. Rev. B **96**, 041202(R) (2017).

[35] O. Türker and S. Moroz, Weyl nodal surfaces, Phys. Rev. B **97**, 075120 (2018).

[36] H. Zhou, C. Peng, Y. Yoon, C. W. Hsu, K. A. Nelson, L. Fu, J. D. Joannopoulos, M. Soljaŭiú, and B. Zhen, Observation of bulk Fermi arc and polarization half charge from paired exceptional points, Science **359**, 1009 (2018).

[37] T. Bzdušek, Q. S. Wu, A. Rüegg, M. Sigrist, and A. A. Soluyanov, Nodal-chain metals, Nature (London) **538**, 75 (2016).

[38] Q. Yan, R. Liu, Z. Yan, B. Liu, H. Chen, Z. Wang, and L. Lu, Experimental discovery of nodal chains, Nat. Phys. **14**, 461 (2018).

[39] B. Song, C. He, S. Niu, L. Zhang, Z. Ren, X.-J. Liu, and G.-B. Jo, Observation of nodal-line semimetal with ultracold fermions in an optical lattice, Nat. Phys. **15**, 911 (2019).

[40] H. Zhou, J. Y. Lee, S. Liu, and B. Zhen, Exceptional surfaces in $\mathcal{PT}$-symmetric non-Hermitian photonic systems, Optica **6**, 190 (2019).

[41] M. Xiao, L. Ye, C. Qiu, H. He, Z. Liu, and S. Fan, Experimental demonstration of acoustic semimetal with topologically charged nodal surface, Sci. Adv. **6**, eaav2360 (2020).

[42] M. Chen, C. Li, G. Palumbo, Y.-Q. Zhu, N. Goldman, and P. Cappellaro, Experimental characterization of the 4D tensor monopole and topological nodal rings, arXiv:2008.00596.

[43] M.-A. Miri and A. Alú, Exceptional points in optics and photonics, Science **363**, eaar7709 (2019).

[44] S. Weimann, M. Kremer, Y. Plotnik, Y. Lumer, S. Nolte, K. G. Makris, M. Segev, M. C. Rechtsman, and A. Szameit, Topologically protected bound states in photonic parity–time-symmetric crystals, Nat. Mater. **16**, 433 (2017).

[45] P. R. Halmos, Normal dilations and extensions of operators, Summ. Bras. Math. **2**, 125 (1950).

[46] C. Sparrow, E. Martin-Lopez, N. Maraviglia, A. Neville, C. Harrold, J. Carolan, Y. N. Joglekar, T. Hashimoto, N. Matsuda, J. L. O'Brien, D. P. Tew, and A. Laing, Simulating the vibrational quantum dynamics of molecules using photonics, Nature (London) **557**, 660 (2018).

[47] See Supplemental Material at http://link.aps.org/supplemental/10.1103/PhysRevLett.127.026404 for experimental details, alternative model with symmetry-protected exceptional lines, further information of intrinsic exceptional lines and robustness of exceptional lines against perturbation, which includes Refs. [48–52].

[48] L. Xiao, K. K. Wang, X. Zhan, Z. H. Bian, K. Kawabata, M. Ueda, W. Yi, and P. Xue, Observation of Critical Phenomena in Parity-Time-Symmetric Quantum Dynamics, Phys. Rev. Lett. **123**, 230401 (2019).

[49] K. K. Wang, X. Qiu, L. Xiao, X. Zhan, Z. H. Bian, W. Yi, and P. Xue, Simulating Dynamic Quantum Phase Transitions in Photonic Quantum Walks, Phys. Rev. Lett. **122**, 020501 (2019).

[50] K. K. Wang, X. P. Wang, X. Zhan, Z. H. Bian, J. Li, B. C. Sanders, and P. Xue, Entanglement-enhanced quantum metrology in a noisy environment, Phys. Rev. A **97**, 042112 (2018).

[51] A. Gilchrist, N. K. Langford, and M. A. Nielsen, Distance measures to compare real and ideal quantum processes, Phys. Rev. A **71**, 062310 (2005).

[52] A. Jamiolkowski, Linear transformations which preserve trace and positive semidefiniteness of operators, Rep. Math. Phys. **3**, 275 (1972).